(Received 26 August 2025, Accepted 3 October 2025, Scheduled 22 October 2025)

A Compact Wideband Circularly Polarized RFID Reader Antenna with a Coupling Inner Ring

Qiaomei Zhang, Wenchao Zhang, and Jiade Yuan*

College of Physics and Information Engineering, Fuzhou University, Fuzhou 350300, China

ABSTRACT: A compact wideband circularly polarized radio frequency identification (RFID) reader antenna with a coupling inner ring is proposed. The antenna consists of a radiating patch, a feeding network, and vertical fences along the sidewalls. The radiating patch incorporates both an outer ring and a coupling inner ring, which significantly broadens the gain bandwidth. Meanwhile, the sidewalls and vertical fences enable directional radiation and contribute to miniaturization. The overall antenna size is 100 mm × 100 mm × 24.6 mm. Measured results show a −10 dB impedance bandwidth of 663–1191 MHz, a 3 dB axial ratio bandwidth of 710–1085 MHz, a 4.5 dBic gain bandwidth of 885–1150 MHz, and a maximum gain of 6.36 dBic. Featuring a compact structure, wide impedance bandwidth, broad axial ratio bandwidth, and enhanced gain performance, the proposed reader antenna is well suited for ultra-high-frequency (UHF) RFID applications, particularly in space-constrained environments or in scenarios where tag antennas are susceptible to frequency deviations.

1. INTRODUCTION

Ultra-high-frequency (UHF) radio frequency identification (RFID) technology, known for its long-range identification, high data throughput, and large storage capacity, has been widely adopted in intelligent logistics, warehouse management, and other related fields [1]. As a key component of RFID systems, the reader antenna directly impacts communication range and system reliability. To address the challenge of reading tag antennas that undergo frequency deviations and meet the needs of space-constrained deployments, reader antenna designs in recent years have increasingly focused on achieving wide bandwidth and compact size.

In practical RFID applications, environmental factors often induce frequency deviations in tag antennas. Wideband reader antennas enhance communication reliability in complex environments by covering the operating frequency range of RFID tags even under such deviation conditions. Considerable research efforts have been dedicated to wideband performance enhancement through various techniques [2–12]. A widely adopted strategy is etching slots into the radiating patch [2–5]. For example, [3, 4] show that slot structures can simultaneously enhance both impedance bandwidth and axial ratio bandwidth by optimizing the surface current distribution. In [5], a dual-fed square microstrip antenna incorporating tilted X-shaped central slits was proposed, achieving a superior axial ratio bandwidth compared to conventional dual-feed designs. Another effective approach is placing parasitic patches around the main radiator. As demonstrated in studies [6–8], parasitic patches introduce multiple resonances, significantly broadening the axial ratio bandwidth. Furthermore, advanced feeding networks have been utilized to improve the impedance bandwidth and circular polarization bandwidth, as reported in [9–12].

The miniaturization of reader antennas is essential in RFID field, as it enables integration into portable devices such as handheld readers, facilitates deployment in space-constrained environments like dense warehouses, and helps to reduce both material consumption and RFID system costs. To meet the increasing demand for compact antenna structures, various miniaturization techniques have been proposed [11–20]. One approach utilizes folded geometries, where reshaping the radiating elements effectively reduces the physical footprint [11–13]. Another method involves using shorting elements, as reported in [13, 14]. Incorporating shorting patches introduces capacitive loading between the radiating patch and ground plane, thereby lowering the resonant frequency and reducing the antenna size. Artificial magnetic conductors (AMCs) have also been employed. Studies [15–17] integrate an AMC layer beneath the antenna, thereby reducing the antenna profile. Lastly, sidewall space utilization, as discussed in [18–20], involves folding the feeding network or radiating structures onto vertical surfaces, thus reducing the antenna's aperture size.

A compact wideband circularly polarized RFID reader antenna featuring a coupling inner ring and vertical fences is proposed in this paper. The inner coupling ring extends the gain bandwidth, while the vertical fences facilitate directional radiation and contribute to overall size reduction.

2. ANTENNA STRUCTURE AND ANALYSIS

2.1. Antenna Configuration

As shown in Fig. 1, the proposed antenna comprises a radiating patch, feeding network, ground plane, and vertical fences, all fabricated on 0.8 mm thick FR4 substrates ($\varepsilon_r = 4.4$ and $\tan\delta = 0.02$).

* Corresponding author: Jiade Yuan (yuanjiade@fzu.edu.cn).

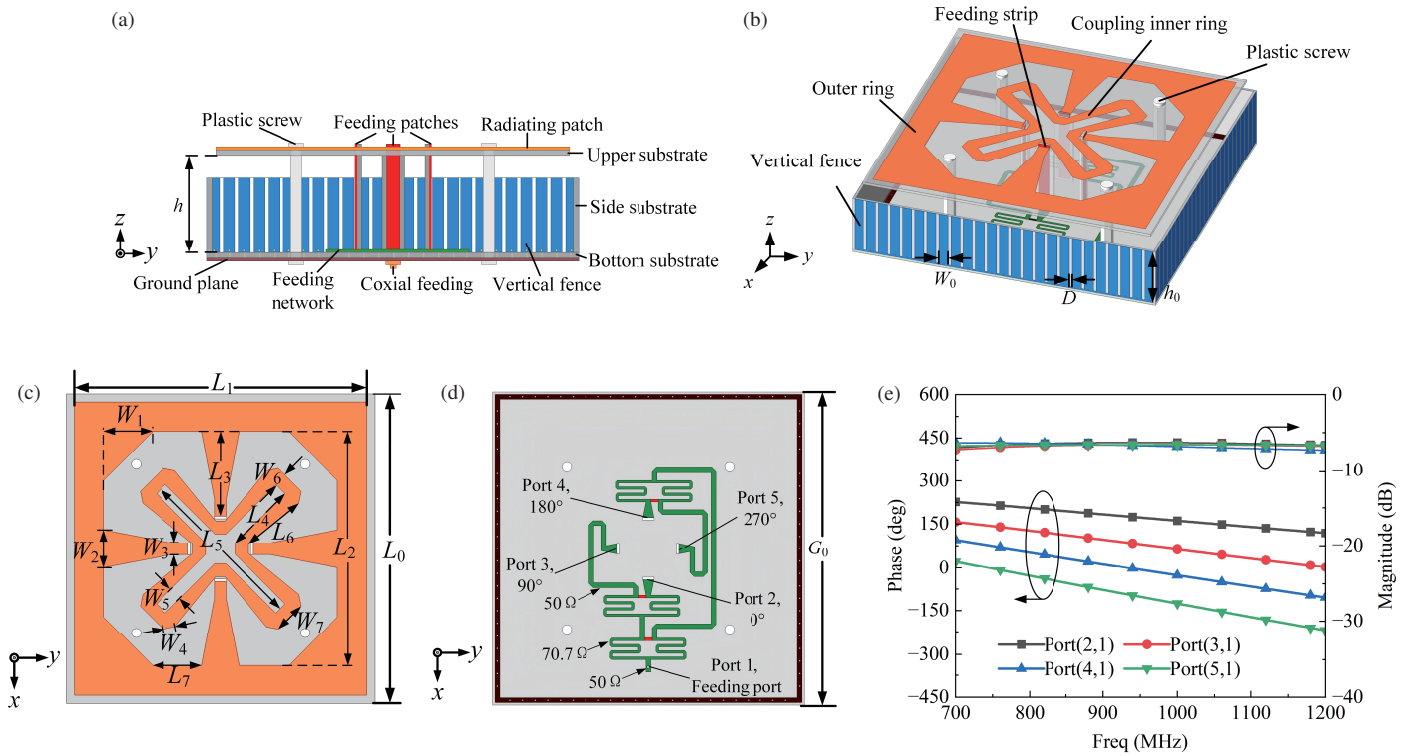

FIGURE 1. Antenna geometry and S-parameters: (a) side view, (b) three-dimensional view, (c) radiating patch, (d) feeding network, (e) simulated S-parameters of feeding network.

TABLE 1. Geometrical parameters of the proposed antenna.

Parameter	Dimension (mm)	Parameter	Dimension (mm)	Parameter	Dimension (mm)	Parameter	Dimension (mm)
G_0	100	D	1	L_5	52	W_3	3.5
L_0	95	L_1	90	L_6	19.91	W_4	3.75
h_0	18.8	L_2	72	L_7	15.25	W_5	4
h	23	L_3	26	W_1	15	W_6	4
W_0	3	L_4	21.64	W_2	11.5	W_7	10

The radiating patch is printed on the upper surface of the top dielectric substrate and consists of an outer ring and a coupling inner ring. The feeding network, formed by three Wilkinson power dividers and phase-shifting lines, is printed on the upper surface of the bottom substrate. The simulated S-parameters of this feeding network are depicted in Fig. 1(e). The feeding network provides four output signals with sequential phase shifts of approximately 0°, 90°, 180°, and 270°. The signal amplitude at each output port is simulated to be around −6.4 dB, slightly below the theoretical value of −6 dB. This discrepancy is attributed to ohmic losses in the microstrip lines and resistors. Vertical fences are printed on the sidewall substrates and connected to the ground plane through metallized vias. Four feeding strips connect the radiating patch to output ports of the feeding network, respectively. The structure is stabilized with four plastic screws. The parameters of the proposed antenna are optimized using ANSYS HFSS, and the final optimized configuration parameters are listed in Table 1.

2.2. Design Analysis

For a typical square ring antenna, resonance occurs when the average perimeter of the ring is equal to an integer multiple of the wavelength [21]. The resonant frequency can be estimated using the following formula [22]:

$$f_n = \frac{nc}{4\left[L_1 - \frac{1}{2}\left(L_1 - L_2\right)\right]\sqrt{\varepsilon_{eff}}}, \quad n = 1, 2, 3 \ldots \tag{1}$$

where c is the speed of light in free space; L_1 and L_2 represent the outer and inner side lengths of the square ring; and ε_{eff} is the effective relative permittivity of the multilayer dielectric substrate. The effective permittivity ε_{eff} of the mixed dual-layer dielectric substrate can be calculated using the following equation [13]:

$$\varepsilon_{eff} = \frac{\varepsilon_{r1}\varepsilon_{r2}\left(h_1 + h_2\right)}{\varepsilon_{r1}h_2 + \varepsilon_{r2}h_1} \tag{2}$$

where ε_{r1} and ε_{r2} denote the relative permittivity of the air layer and the FR4 dielectric substrates, and h_1 and h_2 are their

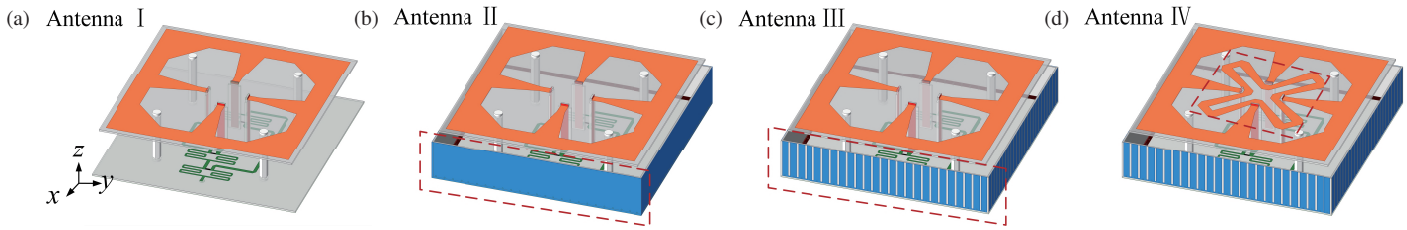

FIGURE 2. Structural evolution process of antenna design: (a) Antenna I, (b) Antenna II, (c) Antenna III, and (d) Antenna IV.

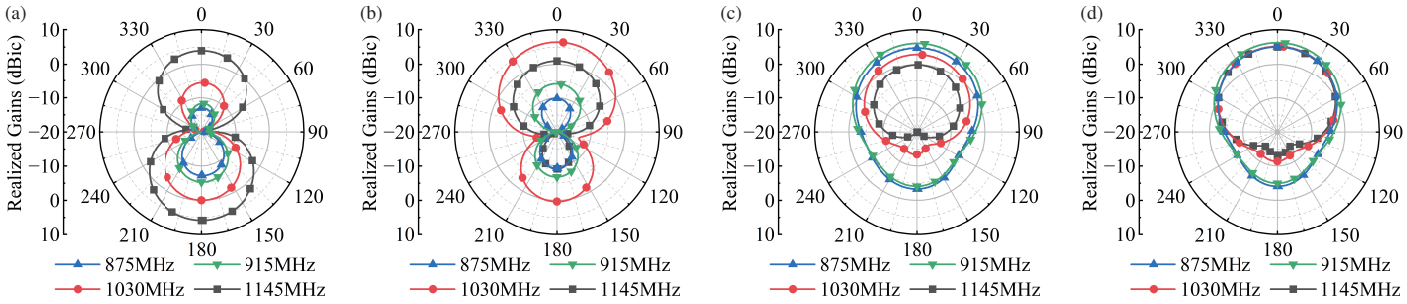

FIGURE 3. Radiation patterns of four antennas: (a) Antenna I, (b) Antenna II, (c) Antenna III, and (d) Antenna IV.

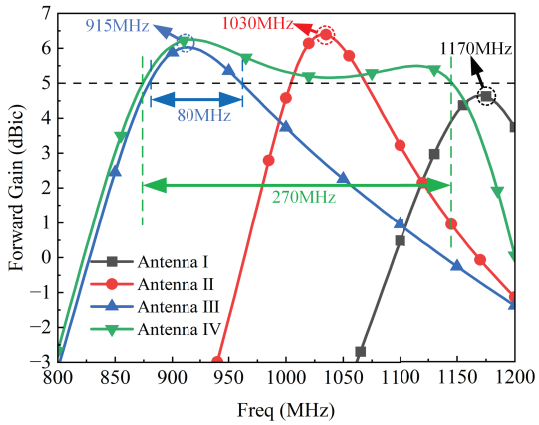

FIGURE 4. Simulated forward gain of four antennas.

corresponding thicknesses. The dielectric substrate of the proposed antenna consists of three layers, including a 23 mm-thick air layer and two FR4 substrates, each with a thickness of 0.8 mm. Accordingly, $\varepsilon_{r1} = 1$, $\varepsilon_{r2} = 4.4$, $h_1 = 23$ mm, and $h_2 = 1.6$ mm. Based on these values, the effective relative permittivity ε_{eff} of the antenna is calculated to be 1.053.

Figure 2 illustrates the evolution of the antenna design. The proposed antenna is derived from a conventional square ring patch antenna, as shown in Antenna I in Fig. 2(a). Based on Antenna I, four copper-clad laminates are vertically loaded around the ground plane to form a reflective cavity, resulting in Antenna II, as depicted in Fig. 2(b). The radiation patterns of Antenna I and Antenna II at different frequencies are shown in Figs. 3(a) and (b), respectively. It can be observed that the directivity of Antenna II is significantly improved, which can be attributed to the reflective cavity that enhances the reflection of upward-propagating electromagnetic waves. Furthermore, as illustrated in Fig. 4, Antenna II demonstrates a higher peak gain than Antenna I, with the resonant frequency exhibiting a downward shift from 1170 MHz to 1030 MHz. The frequency downshift of the peak gain in Antenna II is primarily attributed to the vertical loading structure, which positions the sidewalls closer to the radiating patch. This proximity increases the equivalent capacitive reactance, thereby inducing a low-frequency shift in the resonant frequency.

A series of slots etched into the copper-clad laminates form vertical fences, resulting in Antenna III (Fig. 2(c)). Compared to Antenna II, Antenna III exhibits improved directional radiation patterns, as shown in Figs. 3(b) and (c). Fig. 4 demonstrates a downward shift in the peak gain frequency of Antenna III from 1030 MHz (Antenna II) to 915 MHz. This frequency reduction, facilitated by the integration of vertical fences, directly enables antenna miniaturization. The underlying mechanism is attributed to the periodic boundary conditions introduced by these vertical fences, which induce additional diffraction and scattering of electromagnetic waves. Consequently, the electromagnetic field distribution within the reflective cavity is altered, effectively modulating the resonant frequency of Antenna III. Furthermore, by replacing the fully copper-clad sidewalls of the reflective cavity with a periodic fence structure formed by slotting the copper-clad laminates, the equivalent electrical length of the cavity is increased. This increase in electrical length lowers the resonant frequency, resulting in the downward shift of the peak gain frequency.

Finally, an inner ring is introduced at the center of the radiating patch of Antenna III, resulting in the final design of Antenna IV, as shown in Fig. 2(d). As depicted in Fig. 3(d), Antenna IV exhibits increased forward radiation gain across all four analyzed frequency points. According to Fig. 4, the simulated forward radiation gain exceeds 5 dBic over a broad frequency range of 875–1145 MHz. Compared to Antenna III, the 5 dBic gain bandwidth is significantly extended from 80 MHz to 270 MHz. This improvement is attributed to the inner cou-

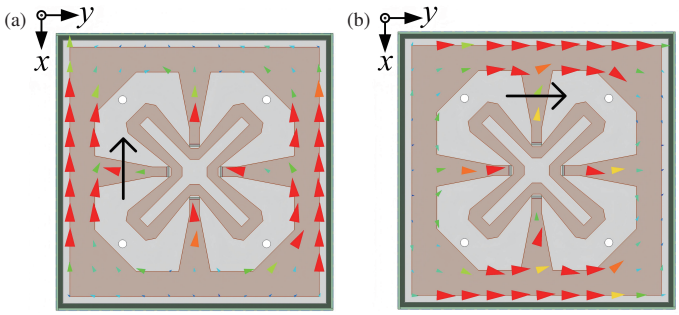

FIGURE 5. Simulated surface current distributions of the radiating patch at 915 MHz. (a) $t = 0$. (b) $t = T/4$.

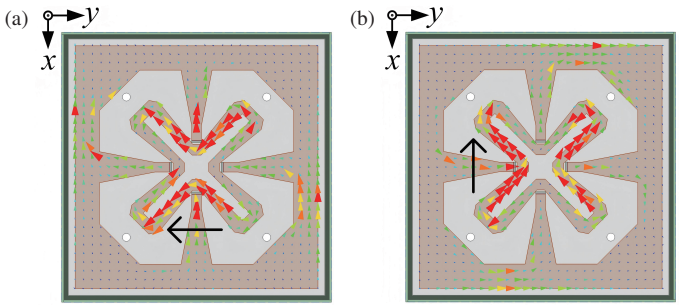

FIGURE 6. Simulated surface current distributions of the radiating patch at 1060 MHz. (a) $t = 0$. (b) $t = T/4$.

pling ring, which introduces an additional high-frequency resonance due to the inner ring's slightly smaller perimeter than the outer ring.

2.3. Circular Polarization Analysis

Left-hand circular polarization (LHCP) is achieved using a feeding network comprising three Wilkinson power dividers and phase-shifting lines. To verify this polarization characteristic, simulated surface current distributions at the boresight for two representative frequencies are illustrated in Figs. 5 and 6.

The surface current distributions on the radiating patch at 915 MHz are shown in Figs. 5(a) and (b) at time instants $t = 0$ and $t = T/4$, respectively. At $t = 0$, the current is predominantly concentrated on the left and right strips of the outer ring, flowing in the $-X$ direction. By $t = T/4$, the current has redistributed to the top and bottom strips of the outer ring, flowing in the $+Y$ direction. Over one complete time period (T), the current sequentially flows in the $-X$, $+Y$, $+X$, and $-Y$ directions, confirming the clockwise rotation of the current at boresight over time. According to classical antenna theory [21], the rotation of surface currents in this antenna generates a far-field electric field that rotates in the same clockwise direction. Therefore, the antenna radiates LHCP waves in the half-space of $z > 0$ at 915 MHz.

The surface current distributions on the radiating patch at 1060 MHz are shown in Figs. 6(a) and (b) at time instants $t = 0$ and $t = T/4$, respectively. At $t = 0$, the current is concentrated on the top and bottom strips of the inner ring, with the resultant equivalent current flowing along the $-Y$ direction. By $t = T/4$, the current redistributes to the left and right strips of the inner ring, and the resultant equivalent current shifts to the $-X$ direction. This behavior confirms that the current also rotates clockwise over time at the boresight. Consistent with the mechanism observed at 915 MHz, this clockwise rotation of surface current verifies that LHCP is similarly realized in the half-space of $z > 0$ at 1060 MHz.

2.4. Parameter Analysis

Figure 7 illustrates the effect of the air gap height (h) on the antenna gain performance. As parameter h increases from 20 mm to 26 mm in 3-mm increments, the antenna gain is observed to improve. This enhancement is primarily due to the increased spacing between the radiating patch and reflective cavity, which enhances radiation efficiency and subsequently elevates the gain. Through a balance between the antenna profile height and gain bandwidth, the optimal air gap h is determined to be 23 mm.

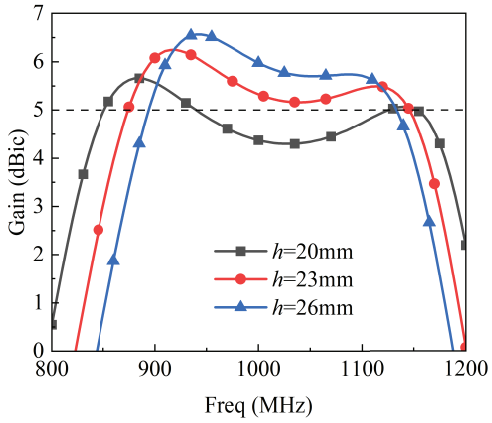

FIGURE 7. Variations in gain with different air gap heights (h).

3. RESULTS AND DISCUSSION

Based on simulation results, a prototype of the antenna is fabricated, as shown in Fig. 8(a). The gain, axial ratio, and radiation patterns are measured in an MVG microwave anechoic chamber. The measurement setup is illustrated in Fig. 8(b).

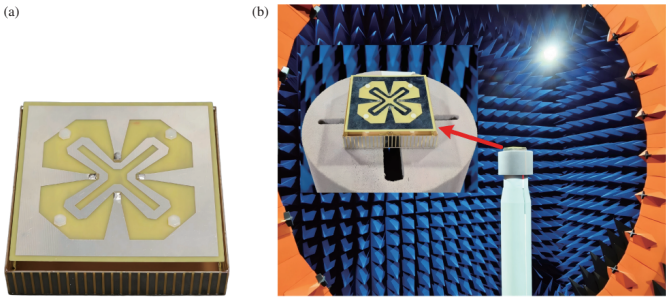

FIGURE 8. (a) Fabricated prototype of the proposed antenna. (b) Measurement setup.

Figure 9 presents comparisons between the simulated and measured results for $|S_{11}|$, axial ratio, and gain. The measured

TABLE 2. Performance comparison with a few previously reported circularly polarized UHF RFID reader antennas.

Ref.	Antenna Size/mm^3	Relative Size/$\lambda_0{}^3$	−10 dB IBW/MHz (Relative IBW)	3 dB AR BW/MHz (Relative AR)	Peak Gain / dBic
This paper	100 × 100 × 24.6	0.305 × 0.305 × 0.075 @915 MHz	663–1191, (56.96%)	710–1085, (41.78%)	6.36
[3]	250 × 250 × 60	0.76 × 0.76 × 0.18 @915 MHz	685–1125, (48.6%)	836–986, (16.5%)	8.6
[10]	210 × 210 × 32.4	0.6 × 0.6 × 0.09 @860 MHz	810–960, (16.9%)	860–930, (7.8%)	8.7
[16]	210 × 210 × 30	0.64 × 0.64 × 0.09 @915 MHz	903–927, (2.6%)	902–950, (5.25%)	3.1
[23]	240 × 240 × 107	0.73 × 0.73 × 0.33 @915 MHz	884–932, (5.3%)	890–934, (4.8%)	9.8
[24]	200 × 200 × 13.2	0.615 × 0.615 × 0.04 @922.5 MHz	906–936, (3.26%)	920–925, (0.54%)	8.65
[25]	140 × 140 × 10.4	0.42 × 0.42 × 0.03 @915 MHz	900–930, (3.3%)	911–922, (1.2%)	7.3
[26]	129.2 × 129.2 × 26	0.37 × 0.37 × 0.075 @867 MHz	854–889, (4.02%)	857–975, (12.88%)	6.45
[27]	180 × 180 × 100	0.54 × 0.54 × 0.30 @915 MHz	820–1230, (40%)	895–970, (7.3%)	6.3
[28]	110 × 110 × 15	0.33 × 0.33 × 0.05 @915 MHz	872–1095, (22.7%)	888–933, (4.9%)	5.52
[29]	60 × 60 × 7.5	0.17 × 0.17 × 0.02 @866.5 MHz	854–877, (2.66%)	862–871, (1.03%)	1.5

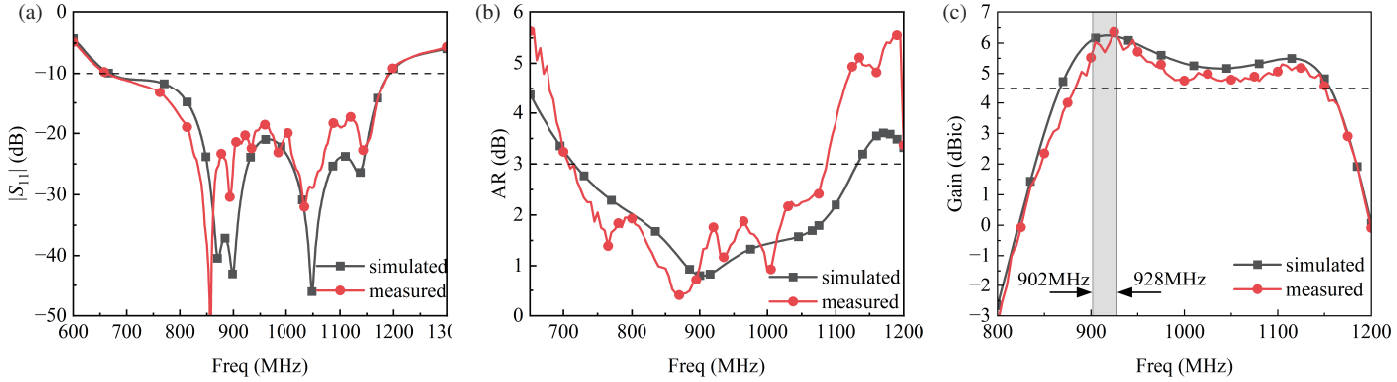

FIGURE 9. Simulated and measured $|S_{11}|$, ARs, and gains of the proposed antenna. (a) $|S_{11}|$. (b) AR. (c) gain.

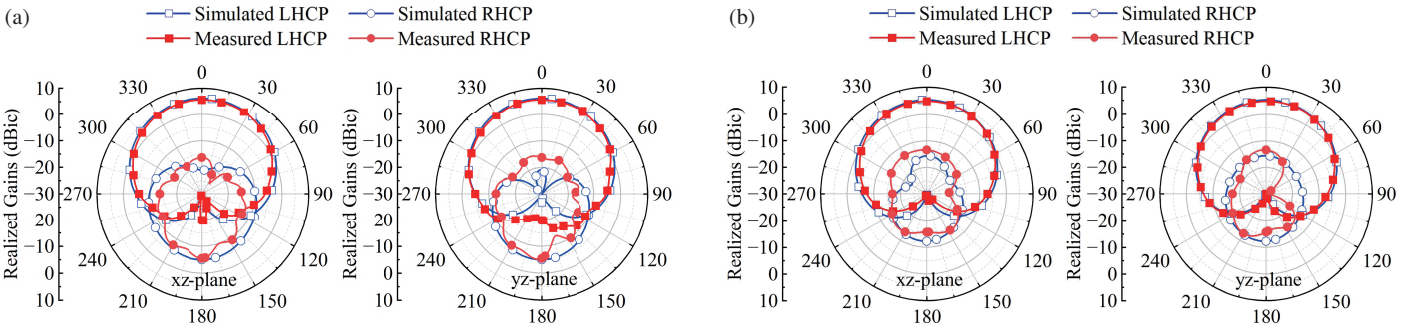

FIGURE 10. Simulated and measured radiation patterns. (a) 915 MHz. (b) 1060 MHz.

results show that the antenna achieves an impedance bandwidth ($|S_{11}| \leq -10$ dB) from 663 MHz to 1191 MHz and a 3 dB axial ratio bandwidth from 710 MHz to 1085 MHz. A peak gain of 6.36 dBic is achieved at 925 MHz. The antenna gain ranges from 5.52 dBic to 6.36 dBic within the North American UHF RFID band (902–928 MHz). The measured gain remains above 4.5 dBic across 885–1150 MHz, confirming the robust performance over a wide frequency range. Due to deviations in the substrate dielectric constant and fabrication-related imperfections, the measured gain is slightly lower than the simulated result, and the measured 4.5 dBic bandwidth remains comparable to the simulated 5 dBic bandwidth.

Figure 10 illustrates the simulated and measured radiation patterns of the proposed antenna in the xz-plane and yz-plane, at 915 MHz and 1060 MHz. The results show good agreement between simulation and measurement, and the antenna exhibits good directional radiation characteristics.

Table 2 compares the performance of the proposed antenna with that of previously reported circularly polarized UHF RFID reader antennas. Notably, the proposed design achieves the

widest impedance bandwidth and axial ratio bandwidth among all referenced antennas. In contrast to the antennas reported in [3, 10, 16, 23, 24], it offers over a 50% size reduction, with a smaller footprint. This enhances its suitability for integration into compact RFID devices. Although the antenna in [25] achieves a gain of 7.3 dBic in a compact size, its axial ratio bandwidth is extremely narrow at only 1.2%. Compared with the designs in [26–28], the proposed antenna provides a similar gain but demonstrates superior performance in terms of size, impedance bandwidth, and axial ratio bandwidth. While the antenna in [29] has a smaller footprint, its gain is approximately 5 dB lower than that of the proposed design.

4. CONCLUSION

This paper presents a compact wideband circularly polarized RFID reader antenna. Directional radiation is achieved through the implementation of vertical fences along the antenna's sidewalls. Additionally, a coupling inner ring embedded within the outer ring effectively broadens the gain bandwidth. The antenna is fabricated on FR4 substrates and occupies a compact volume of 100 mm $\times$ 100 mm $\times$ 24.6 mm. Measured results show a -10 dB impedance bandwidth of 56.96% and a 3 dB axial ratio bandwidth of 41.78%. The measured gain remains above 4.5 dBic over the 885–1150 MHz range, with a peak gain of 6.36 dBic achieved at 925 MHz. Owing to its low cost, compact size, relatively high gain, and wide axial ratio bandwidth, the proposed reader antenna is an excellent candidate for UHF RFID reader applications, particularly in scenarios where tag antennas are susceptible to frequency deviations and in space-constrained environments.

ACKNOWLEDGEMENT

This work was supported in part by the University-Industry Research Collaboration Program of Fujian Province, China, under Grant 2023H6004.

REFERENCES

[1] Liu, Q., J. Shen, H. Liu, Y. Wu, M. Su, and Y. Liu, "Low-cost compact circularly polarized directional antenna for universal UHF RFID handheld reader applications," *IEEE Antennas and Wireless Propagation Letters*, Vol. 14, 1326–1329, 2015.

[2] Ata, O. W., M. Salamin, and K. Abusabha, "Double U-slot rectangular patch antenna for multiband applications," *Computers & Electrical Engineering*, Vol. 84, 106608, 2020.

[3] Sim, C.-Y.-D., Y.-W. Hsu, and G. Yang, "Slits loaded circularly polarized universal UHF RFID reader antenna," *IEEE Antennas and Wireless Propagation Letters*, Vol. 14, 827–830, 2015.

[4] Li, J., H. Liu, S. Zhang, M. Luo, Y. Zhang, and S. He, "A wideband single-fed, circularly-polarized patch antenna with enhanced axial ratio bandwidth for UHF RFID reader applications," *IEEE Access*, Vol. 6, 55 883–55 892, 2018.

[5] Ata, O. W., "A circularly polarized microstrip antenna with dual feed and tilted slit X-shaped geometry," *International Journal of Microwave and Optical Technology*, Vol. 11, No. 6, 444–452, Nov. 2016.

[6] Feng, G., L. Chen, X. Wang, X. Xue, and X. Shi, "Broadband circularly polarized crossed bowtie dipole antenna loaded with parasitic elements," *IEEE Antennas and Wireless Propagation Letters*, Vol. 17, No. 1, 114–117, 2018.

[7] Wu, R., J.-H. Lin, J.-F. Li, and F.-C. Chen, "Wideband circularly polarized antenna with novel asymmetric Y-shaped arms," *IEEE Antennas and Wireless Propagation Letters*, Vol. 23, No. 4, 1181–1185, 2024.

[8] Chen, Z., J. Zeng, S. Xu, and J. Wang, "Compact ultra-wideband circularly polarized crossed-dipole antenna with post fence and parasitic elements," *IEEE Antennas and Wireless Propagation Letters*, Vol. 23, No. 10, 3168–3172, 2024.

[9] Xu, R., J. Liu, K. Wei, W. Hu, Z.-J. Xing, J.-Y. Li, and S. S. Gao, "Dual-band circularly polarized antenna with two pairs of crossed-dipoles for RFID reader," *IEEE Transactions on Antennas and Propagation*, Vol. 69, No. 12, 8194–8203, 2021.

[10] Doan, T. N. H., H. D. Le, V. S. Hoang, K. K. Nguyen, and S. X. Ta, "A low-profile broadband circularly polarized slot antenna loaded with metasurface for UHF-RFID readers," *IEEE Access*, Vol. 13, 93 057–93 062, 2025.

[11] Ren, J., H. Liu, Y. Zeng, Z. Wang, and S. Fang, "Dual-band circularly polarized antenna with wide axial-ratio and gain beamwidths for high-precision BDS applications," *Progress In Electromagnetics Research C*, Vol. 145, 63–74, 2024.

[12] Wei, K., J. Liu, R. Xu, W. Hu, C. Chen, W. Jiang, and S. Gao, "A dual-band rotational feed circularly polarized RFID reader antenna array with stable gain," *IEEE Antennas and Wireless Propagation Letters*, Vol. 24, No. 7, 1620–1624, 2025.

[13] Yuan, J., J. Zheng, and Z. D. Chen, "A compact meandered ring antenna loaded with parasitic patches and a slotted ground for global navigation satellite systems," *IEEE Transactions on Antennas and Propagation*, Vol. 66, No. 12, 6835–6843, 2018.

[14] Ma, B., J. Pan, S. Huang, S. Liu, T. Ngo, Z. T. Aung, and Y.-X. Guo, "Compact dual-polarized antenna with enlarged effective-to-physical aperture ratio for wireless power transfer and RFID," *IEEE Transactions on Antennas and Propagation*, Vol. 69, No. 7, 4166–4171, 2021.

[15] Elzuwawi, H. H., M. M. Tahseen, G. H. Elzwawi, and T. A. Denidni, "A new RFID monopole antenna using a compact AMC structure," *Microwave and Optical Technology Letters*, Vol. 61, No. 7, 1835–1840, 2019.

[16] Sarkar, S. and B. Gupta, "A dual-band circularly polarized antenna with a dual-band AMC reflector for RFID readers," *IEEE Antennas and Wireless Propagation Letters*, Vol. 19, No. 5, 796–800, 2020.

[17] Chenaoui, S., L. Mouffok, S. Hebib, A. Fattouche, D. Allane, and S. Tedjini, "Gain stability improvement of a wideband antenna using an artificial magnetic conductor," *Microwave and Optical Technology Letters*, Vol. 65, No. 8, 2267–2277, 2023.

[18] Lou, T., Z. Shen, and X.-X. Yang, "Circularly polarized UWB antenna based on a single-folded substrate," *IEEE Antennas and Wireless Propagation Letters*, Vol. 23, No. 7, 2195–2199, 2024.

[19] Liu, X., Y. Zhu, and W. Xie, "A miniaturized wideband directional circularly polarized antenna based on bent Vivaldi antenna structure," *IEEE Antennas and Wireless Propagation Letters*, Vol. 22, No. 2, 298–302, 2023.

[20] Yang, H., G. Zhao, J. Jiang, T. Liu, L. Zhao, Y. Li, Y. Cai, and J. Yao, "Aperture reduction using downward and upward bending arms for dual-polarized quadruple-folded-dipole antennas," *IEEE Antennas and Wireless Propagation Letters*, Vol. 22, No. 3, 645–649, 2023.

[21] Balanis, C. A., *Antenna Theory: Analysis and Design*, John Wiley & Sons, 2016.

[22] Liu, J.-C., B.-H. Zeng, L. Badjie, S. Drammeh, S.-S. Bor, T.-F. Hung, and D.-C. Chang, "Single-feed circularly polarized

aperture-coupled stack antenna with dual-mode square loop radiator," *IEEE Antennas and Wireless Propagation Letters*, Vol. 9, 887–890, 2010.

[23] Pan, Y. and Y. Dong, "Circularly polarized stack Yagi RFID reader antenna," *IEEE Antennas and Wireless Propagation Letters*, Vol. 19, No. 7, 1053–1057, 2020.

[24] Pimpison, C. and K. Nuangwongsa, "Design of circularly polarized rounded corner square patch antenna with shallow slot for UHF RFID reader applications," in *2024 21st International Conference on Electrical Engineering/Electronics, Computer, Telecommunications and Information Technology (ECTI-CON)*, 1–4, Khon Kaen, Thailand, 2024.

[25] Li, J., G. Huang, C. Yu, M. Zheng, and H. Liu, "A compact circularly polarized ring patch antenna for RFID reader application," in *2024 Photonics & Electromagnetics Research Symposium (PIERS)*, 1–4, Chengdu, China, 2024.

[26] Akdag, I., C. Gocen, M. Palandoken, and A. Kaya, "A novel circularly polarized reader antenna design for UHF RFID applications," *Wireless Networks*, Vol. 28, No. 6, 2625–2636, 2022.

[27] Xue, F., Y. Zhang, J. Li, and H. Liu, "Circularly polarized cross-dipole antenna for UHF RFID readers applicated in the warehouse environment," *IEEE Access*, Vol. 11, 38 657–38 664, 2023.

[28] Wu, S., J. Yuan, J. Chen, and Y. Li, "Compact circularly polarized microstrip ring antenna using capacitive coupling structure for RFID readers," *IEEE Access*, Vol. 8, 32 617–32 623, 2020.

[29] Colella, R., A. Michel, and L. Catarinucci, "Compact 3-D-printed circularly polarized antenna for handheld UHF RFID readers," *IEEE Antennas and Wireless Propagation Letters*, Vol. 17, No. 11, 2021–2025, 2018.